Experimental observation of a phase transition in the evolution of many-body systems with dipolar interactions

Gonzalo A. Álvarez*
Department of Chemical Physics, Weizmann Institute of Science, 76100, Rehovot, Israel

Dieter Suter†
Fakultät Physik, Technische Universität Dortmund, D-44221, Dortmund, Germany

Robin Kaiser‡
Institut Non-Linéaire de Nice, CNRS, Universite de Nice Sophia Antipolis, 06560, Valbonne, France
(Dated:)

arXiv:1409.4562v1 [quant-ph] 16 Sep 2014

Non-equilibrium dynamics of many-body systems is important in many branches of science, such as condensed matter, quantum chemistry, and ultracold atoms. Here we report the experimental observation of a phase transition of the quantum coherent dynamics of a 3D many-spin system with dipolar interactions, and determine its critical exponents. Using nuclear magnetic resonance (NMR) on a solid-state system of spins at room-temperature, we quench the interaction Hamiltonian to drive the evolution of the system. The resulting dynamics of the system coherence can be localized or extended, depending on the quench strength. Applying a finite-time scaling analysis to the observed time-evolution of the number of correlated spins, we extract the critical exponents $\nu \approx s \approx 0.42$ around the phase transition separating a localized from a delocalized dynamical regime. These results show clearly that such nuclear-spin based quantum simulations can effectively model the non-equilibrium dynamics of complex many-body systems, such as 3D spin-networks with dipolar interactions.

The complexity of many-body systems is a long standing problem in physics (1–8). As an example, quantum states of many-body systems can be localized at well defined positions in space or they can be delocalized, depending on parameters like disorder. In their localized regime, such systems may not reach a thermal state but retain information about their initial state on very long timescales (9–17). The role of the topology, dimension, long and short range interactions, and the presence of disorder is very important for the onset of these localization regimes. Much progress was achieved on the numerical and theoretical side, where these phenomena have been predicted under certain conditions. However, experimentally addressing 3D many-body systems in a controlled manner poses severe experimental problems (5, 8, 14, 16). Non-equilibrium dynamics of many-body systems has been investigated to provide complementary information about a large variety of situations but also remains challenging (18–26). Therefore, finding different experimental situations, new approaches and techniques for controlling and observing many-body dynamics can lead to new approaches for studying many-body physics.

The recent progress on the experimental control of cold atoms (6, 27, 28), trapped ions (25, 26, 29, 30), Rydberg atoms (31), polar molecules (7, 32) and nitrogen-vacancy centers in diamond (33–36) has led to promising new ways of studying the non-equilibrium dynamics and localization phenomena of many-body systems. In particular a lot of effort is focused on studying many-spin systems with dipolar interactions of the Heisenberg-type (8, 24–26, 31, 32). Here, we use nuclear magnetic resonance (NMR), which provides a natural and versatile approach for coherently controlling large numbers of spins (up to ~ 7000) in solid state systems, where dipolar interactions are present. NMR techniques allow to quantify the number of spins that are coherently correlated, and allow control of the interaction types and strengths of the Hamiltonians (37–39).

We exploited these advantages to quench the system Hamiltonian, i.e. to suddenly change the interaction Hamiltonian in such a way that its symmetry changes and the previous equilibrium density operator becomes a superposition state that evolves in time under the new Hamiltonian. This evolution generates correlations between the spins. We measure the temporal evolution of the spatial extent of the resulting spin clusters. We adapted the powerful finite-time scaling technique (40, 41) to study the long-time regime of the evolution of the size of correlated spin clusters. For a critical value of a controlled perturbation on the strength of the quench, we show that this many-body system in 3D spin-networks, with competing dipolar interactions that depend on the distance between spins as $1/r^3$ (38, 39), undergo a critical transition from extended to localized dynamics.

System and experimental setup

Our experimental system consists of the ^{1}H nuclear spins of polycrystalline adamantane (Fig. 1, inset). All experiments were performed on a home-built solid-state NMR spectrometer in a magnetic field of 7 Tesla. The interaction of the proton spins $I = 1/2$ with the static magnetic field results in a Zeeman splitting of $\omega_z = 300$ MHz (in frequency units), which is identical for all spins. The mutual

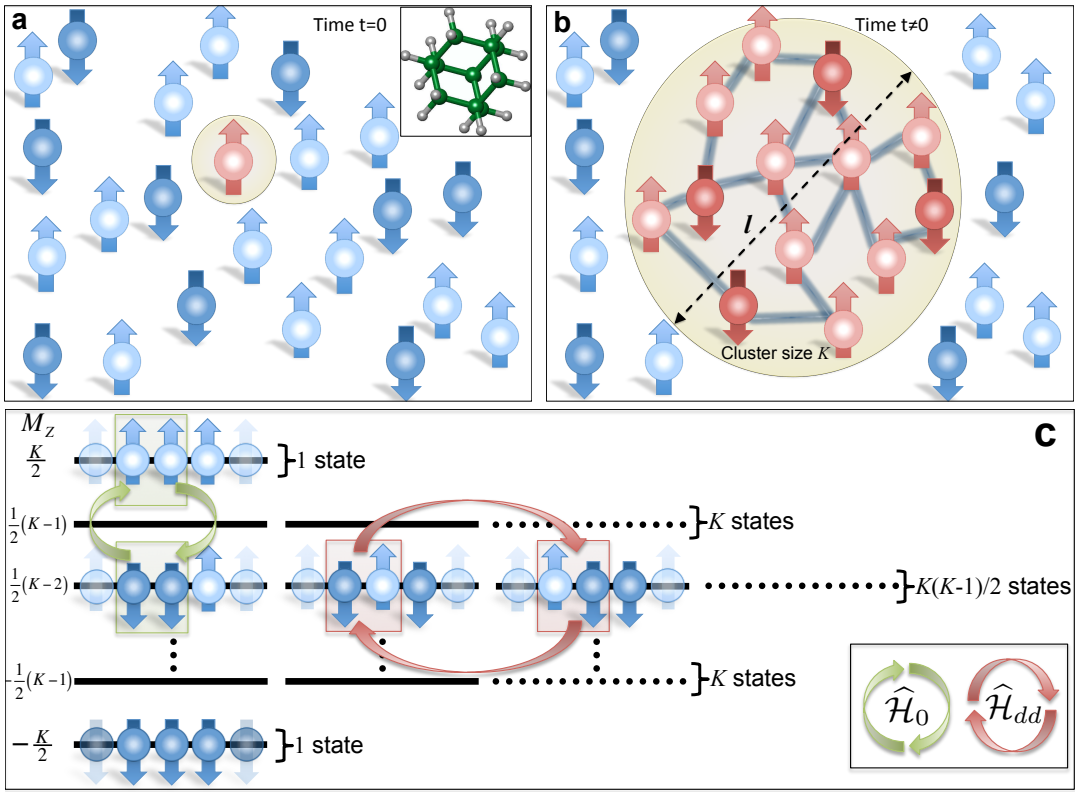

Figure 1. **Quantum evolutions and Hamiltonian characteristics. (A)** Thermal equilibrium of the proton spins in the presence of a static magnetic field at time $t = 0$ just before the quench. The spins are uncorrelated, the density operator is $\hat{\rho}_0 \propto \hat{I}_z = \sum_i \hat{I}_z^i$, where $\hat{I}_z$ is the total spin magnetization operator and $\hat{I}_z^i$ the single spin operators. The red spin in the center represents an uncorrelated spin state $\hat{I}_z^i$ of the spin ensemble. It thus represents a cluster of correlated spins with size $K = 1$. Inset: Adamantane molecule with 16 protons (small gray spheres). The large green spheres represent carbon atoms, consisting of 99 % ^{12}C and 1 % ^{13}C . **(B)** Cluster of correlated spins at time $t > 0$ after the quench with $\widehat{\mathcal{H}}_0$ (red spins). The cluster consisting of $K > 1$ correlated spins occupies a volume l^3, where l is the effective "coherence length". **(C)** Evolution of a system of K spins in the Zeeman product basis $|\alpha_1, \alpha_2, ..., \alpha_K\rangle$ ($\alpha_i = \uparrow, \downarrow$) (black solid lines), where $\hat{I}_z |\alpha_1, \alpha_2, ..., \alpha_K\rangle = M_z |\alpha_1, \alpha_2, ..., \alpha_K\rangle$. The green arrows represent the $\widehat{\mathcal{H}}_0$ interactions, which flips simultaneously two spins and, accordingly, M_z changes by $\Delta M_z = \pm 2$. The red arrow represents the $\widehat{\mathcal{H}}_{dd}$ interactions that conserve the quantum number M_z.

dipole-dipole interactions between the spins corresponds to a 3D spin-coupling network (Fig. 1). The dipolar interaction scales with $1/r^3$ and leads to a resonance width of 7.9 kHz of the NMR spectrum due to the homogeneous broadening (See Ref. (39) for details of the sample). The spin system is initially left to reach thermal equilibrium at room temperature. Its density operator can be then described in this high-temperature limit as $\hat{\rho}_0 \propto \hat{I}_z = \sum_i \hat{I}_z^i$ (37), considering that the Zeeman interaction is much stronger than the dipolar one ($\omega_z = 300$ MHz $\gg 7.9$ kHz). $\hat{I}_z$ is the total spin operator component in the direction of the magnetic field, and $\hat{I}_z^i$ that of the i^{th} spin.

Experimental method and quantum quench

The spin-spin interaction Hamiltonian of the system in a reference frame rotating at the Zeeman frequency is

$$\widehat{\mathcal{H}}_{dd} = \sum_{i<j} d_{ij} \left[2\hat{I}_z^i \hat{I}_z^j - (\hat{I}_x^i \hat{I}_x^j + \hat{I}_y^i \hat{I}_y^j) \right]. \qquad (1)$$

This is the secular part of the dipolar interaction, which commutes with the much stronger Zeeman Hamiltonian ($|\omega_z| \gg |d_{ij}|$). The coupling constants are

$$d_{ij} = \frac{1}{2} \frac{\gamma^2 \hbar^2}{r_{ij}^3} \left(1 - 3\cos^2 \theta_{ij}\right), \qquad (2)$$

with γ the gyromagnetic ratio, θ_{ij} the angle between the internuclear vector $\vec{r}_{ij}$ and the magnetic field direction (37). This Heisenberg-type Hamiltonian is of growing interest in the context of quantum information and simulation science (8, 24–26, 31, 32).

The initial condition corresponds to a thermal equilibrium with uncorrelated spins and the density operator $\hat{\rho}_0$ commutes with the system Hamiltonian $\widehat{\mathcal{H}}_{dd}$ (Fig. 1a). To generate spin clusters of correlated spins, we quench the system by suddenly changing its Hamiltonian to

$$\widehat{\mathcal{H}}_0 = -\sum_{i<j} d_{ij} \left[\hat{I}_x^i \hat{I}_x^j - \hat{I}_y^i \hat{I}_y^j \right], \qquad (3)$$

which does not commute with the thermal equilibrium state (Fig. 1b). We use a method developed by Pines and coworkers (42, 43) based on a sequence of $\pi/2$-pulses that act equally on all spins to generate this effective Hamiltonian.

To study the impact of the quench and monitor the generation of clusters of correlated spins, we compare its evolution under a parametric set of Hamiltonans:

$$\widehat{\mathcal{H}} = (1-p)\widehat{\mathcal{H}}_0 + p\widehat{\mathcal{H}}_{dd}. \tag{4}$$

These Hamiltonians are generated as effective Hamiltonians by letting the system evolve under a periodic sequence of the Hamiltonians $\widehat{\mathcal{H}}_0$, for a duration τ_0 and $\widehat{\mathcal{H}}_{dd}$ for a duration τ_d, resulting in a cycle time $\tau_c = \tau_0 + \tau_{dd}$. The control parameter $p = \tau_{dd}/\tau_c$, defines a perturbation to the quench strength. If $p = 1$, there is no quench, and $1 - p$ defines the strength of the quench. The two Hamiltonians $\widehat{\mathcal{H}}_0$ and $\widehat{\mathcal{H}}_{dd}$ have distinctive symmetries with respect to the total magnetic quantum number M_z, the eigenvalue of $\hat{I}_z$. While the Hamiltonian $\widehat{\mathcal{H}}_0$ flips simultaneously two spins and, accordingly, changes M_z by $\Delta M_z = \pm 2$ (green arrows in Fig. 1c), $\widehat{\mathcal{H}}_{dd}$ mixes states that conserve M_z (red arrows in Fig. 1c).

Growth of the clusters

After the quench, the Hamiltonians (4) generate correlations between the different spins. We measure the average number of correlated spins in the system (the cluster size) by decomposing the corresponding density operator according to its symmetry under rotations around the z-axis, adapting the method of Baum *et al.* (43). From the distribution of coherences of the density matrix as a function of the quantization number ΔM_z (38, 39), we determine the average number of correlated spins K in the generated clusters (see Methods). We associate them to an effective volume l^3, with l the effective correlation length (Fig. 1b). Figure 2a shows the determined cluster size K as a function of the evolution time $t = N\tau_c$ for different perturbation strengths on time scales much shorter than the time required for the system to thermalize. For the unperturbed evolution (black squares), the cluster size grows indefinitely within the time range measured before the experimental signal disappears due to decoherence processes (38, 39). This changes qualitatively when the perturbation is turned on: the growth of the clusters generated by the perturbed Hamiltonian (colored symbols in Fig. 2a) does not continue indefinitely, but saturates at a certain level, to which we refer as the localization size. This localization size decreases with increasing perturbation strength p.

Finite-time scaling

To quantitatively analyze the transition from the delocalized to the localized dynamical regimes, we exploit the powerful finite-time scaling technique (40, 41). Without perturbation the cluster-size is expected to grow with a power law in agreement with several experimental observations in solid-state spin-networks (44). In our system, this growth law is also observed for times $t \gtrsim 0.7$ms and vanishing perturbation $p = 0$, where $K \propto t^{4.3}$ (38, 39). Thus, $K^{2/3} \sim l^2 \sim Dt^{\alpha}$, where D is a generalized diffusion coefficient and α is the exponent of the "diffusion" process (44, 45). In the presence of a critical transition at p_c, which is the perturbation at which a transition from a localized to a delocalized phase occurs, one expects that the cluster-size evolution will depend on $p - p_c$ (40, 41, 45). We use the single-parameter Ansatz for the scaling behavior at long times

$$K^{2/3} \sim t^{k_1} F\left[(p_c - p)\, t^{k_2}\right], \tag{5}$$

where $F(x)$ is an arbitrary function and k_1 and k_2 are constant parameters. We assume that $D(p) \propto (p_c - p)^s$, such that the diffusion coefficient vanishes, $D = 0$, at the onset of the localized regime for $p = p_c$, with s as a critical exponent of the delocalized phase.

In the localized regime, we found experimentally that the localization cluster-size follows a power law on the perturbation strength p (38, 39). Therefore we assume that at long times $K^{2/3} \sim (p - p_c)^{-2\nu}$ for $p > p_c$, as typically assumed for localization phenomena and ν is the critical exponent for the localized phase (40, 41, 45). We performed the finite-time scaling analysis and found the universal scaling for $s \approx \nu$ shown in Fig. 2b,c (see Methods and SI).

The scaling factor $\xi(p)$ that leads to the universal scaling behavior $f\left(\xi(p)\, t^{-k_2\nu}\right) = K^{2/3} t^{-k_1}$, with $f(x)$ an arbitrary function, is shown in Fig. 3 as the blue triangles. The solid red line is a fit with the expression $\xi(p) = \left(A\,|p - p_c|^{\nu} + B\right)^{-1}$, where B accounts for decoherence processes that smooth the critical transition (40, 41). We thus obtain a critical perturbation strength of $p_c = 0.0266 \pm 0.0004$ and the critical exponents $\nu = s = 0.42 \pm 0.07$. We can see the consistency with the scaling law assumptions of Eq. (5). The insets in Fig. 3 show the probability distribution of coherences in the density matrix (see Methods) as a function of the coherence order ΔM_z and the evolution time in both regimes. While for a perturbation strengths $p < p_c$, the coherence distribution spreads indefinitely (delocalized regime), for $p > p_c$ the coherence distribution becomes localized after a given time.

Discussion

From the power law coefficient $\alpha_{exp} \approx 2.86$ experimentally determined in the unperturbed free diffusion regime, we obtain a critical behavior on the transition from the localized to the delocalized regime with critical exponents $s \approx \nu$. This is consistent with Wegner's scaling law $s = (d-2)\nu$ for a three dimensional system ($d = 3$) (46), in agreement with the assumption that the cluster-size K determines an effective volume occupied by the correlated spins and its respective effective correlation length,

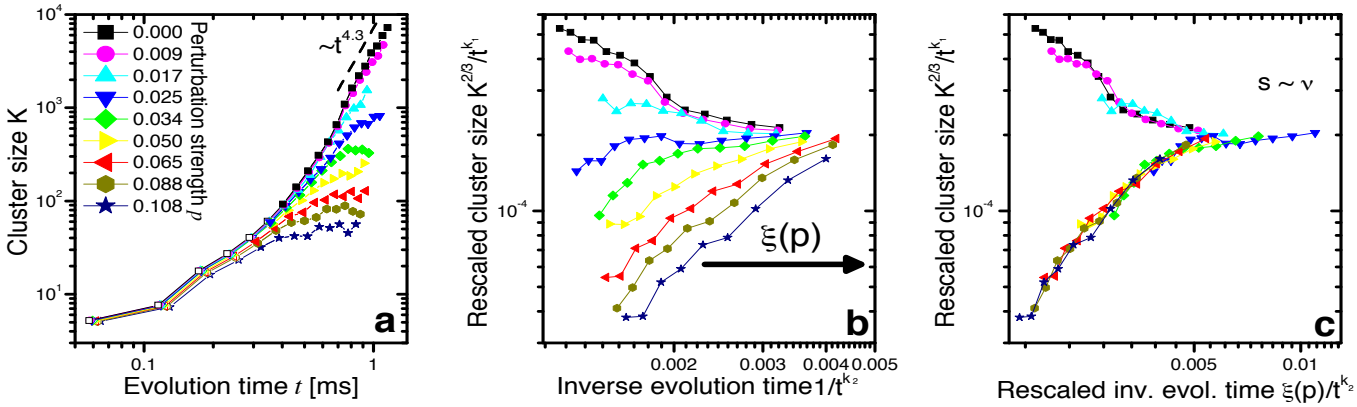

Figure 2. **Time evolution of the cluster size K for different perturbation strengths and finite-time scaling procedure. (A)** Cluster-size K as a function of the time t after the quench. The unperturbed quenched evolution (black squares) shows a cluster-size K that grows as $\sim t^{4.3}$ at long times (dashed line as a guide to the eye). The solid symbols show the points used for the finite-time scaling analysis, while the empty symbols do not belong to the long time regime. For the largest perturbation strengths, localization effects are clearly visible by the saturation of the cluster size. **(B,C)** These two panels represent the finite-time scaling procedure. In (b), the rescaled and squared "correlation length" $l^2/t^{k_1^{exp}} = K^{2/3}(t)/t^{k_1^{exp}}$ as a function of the evolution time $1/t^{k_2^{exp}}$ is plotted, where $k_1^{exp} \approx 1.91$ and $k_2^{exp} \approx 0.96$ were determined using the experimentally measured $\alpha_{exp} \approx 2.87$. In (c), the curves of (b) are shifted horizontally by the scaling factor $\xi(p)$ to obtain a universal scaling law. The rescaled experimental data of $K^{2/3}(t)/t^{k_1^{exp}}$ is shown as a function of $\xi(p)/t^{k_2^{exp}}$, where all curves overlap in a universal curve evidencing the scaling behavior.

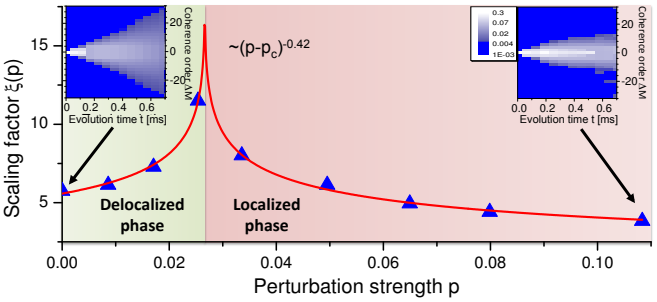

Figure 3. **Scaling factor and critical exponents.** Normalized scaling factor $\xi(p)$ as a function of p (blue triangles). The normalization is based on equalizing $\xi(p = 0.108) = K_{loc}^{1/3} \approx (56.33)^{1/3}$ (see Methods). The red solid line is a fit to the blue triangles with the expression $\xi(p) = \left(A|p - p_c|^{\nu} + B\right)^{-1}$, where $A = 0.58 \pm 0.08$, $B = 0.05 \pm 0.02$, the critical exponent $\nu = 0.42 \pm 0.07$ and the critical perturbation $p_c = 0.0266 \pm 0.0004$. From Fig. 2 we determined that $\nu \approx s$. The two insets show the distribution of coherence orders of the density matrix as a function of the evolution time t for the perturbation strengths $p = 0$ and $p = 0.108$, which correspond to the delocalized and localized regime, respectively. The corresponding scaling factors are indicated by the arrows.

$l^3 \propto K$. While a microscopical derivation should be developed to confirm our findings, the present results represent strong evidence of a critical transition in the coherence length of our system after the quench. This critical behavior is induced by competing dipole-dipole interactions in the many-body dynamics of the cluster of correlated spins.

Conclusion

We developed a method to experimentally monitor the dynamics of many-body systems in 3D spin-networks with competing dipole-dipole interactions with different symmetries. By quenching the system with a Hamiltonian that creates clusters of correlated spins, we determine the effective correlation length of the growing clusters. Regulating the quenching strength by adding as perturbation the raw thermalizing Hamiltonian, we induced localization effects in a controlled way. We exploited a finite-time scaling approach (40, 41) to determine the scaling law for the long-time behavior of the cluster-size growth. This allowed us to identify a sharp transition in the dynamical behavior of the cluster size, which we interpret as a phase transition from a delocalized to a localized coherent dynamical regime. We quantified the critical exponents for both phases and found them to be indistinguishable, both ~ 0.42. Our results show on one side that NMR can be used as another front line for distilling the physics of localization and non-equilibrium phenomena in many-body systems, and on the other side they provide a new general approach that can be implemented also by other communities interested in these outstanding problems.

Materials and methods

Determination of the size of clusters of correlated spins

$\widehat{\mathcal{H}}_0$ drives an evolution that converts the thermal initial state into a density operator containing terms of

the form $\hat{I}_u^i ... \hat{I}_v^j \hat{I}_w^k$ $(u, v, w = x, y, z)$, where the indexes i, j, k identify the spins involved in a cluster of correlated spins. The cluster-size K corresponds to the number of terms in this product, which is equal to the number of correlated spins.

As the Hamiltonian $\widehat{\mathcal{H}}_0$ flips simultaneously two spins and, $\Delta M_z = \pm 2$ (green arrows in Fig. 1), at the same time, the number K of correlated spins changes by $\Delta K = \pm 1$. This evolution generates a density operator only containing elements ρ_{ij} with $\Delta M_z = M_z(i) - M_z(j) = 2n$, $n = 0, 1, 2 \ldots$. Such elements ρ_{ij} are called ΔM_z quantum coherences and can be quantified by the multiple quantum coherence (MQC) spectrum $A(\Delta M_z)$ given by the amplitude of coherences of the density matrix for a given ΔM_z (38, 39, 43). The time evolution of the MQC spectrum is shown in the insets of Fig. 3 for $p = 0$ and $p = 0.108$. $\rho(t = 0) = \rho_0$ is diagonal and then $A(\Delta M_z) \neq 0$ only for $\Delta M_z = 0$, but as higher coherence orders are excited during the evolution, $A(\Delta M_z)$ spreads, thus manifesting the increasing cluster size. We determined the average number of correlated spins in the generated clusters by the half width at e^{-1} of the coherence distribution $A(\Delta M_z)$ (43): $\sigma = \sqrt{K}$ (see (38, 39) for details).

Finite size scaling analysis

From the condition that at long times $K^{2/3} \sim (p_c - p)^s t^\alpha$ for $p < p_c$ and $K^{2/3} \sim (p - p_c)^{-2\nu}$ for $p > p_c$, one obtains that $k_1 = \frac{2\nu\alpha}{2\nu+s}$ and $k_2 = \frac{\alpha}{2\nu+s}$. We performed the finite-time scaling analysis for different relations between the two critical exponents, i.e. varying β on the relation $s = \beta\nu$, and we found the best scaling behavior for $s = \nu$ (see SI). We then found the scaling factor $\xi(p)$ for each case, by horizontally shifting the curves of Fig. 2b to overlap with each other for different values of p in such a way that they generate a single curve as in Fig. 2c. This is only possible if the single parameter scaling Eq. (5) is consistent with the experimental data, thus confirming the single parameter hypothesis. The shifting procedure is invariant under a global shift of the origin for $\xi(p)$. To determine the absolute scale, we used the experimental data from the localization regime, for the largest perturbation strength, where the localization is clearly evident (stars in Fig. 2). In the localized regime $p > p_c$, $K(t \to \infty) = K_{loc}$ and therefore $f\left(\xi(p)\, t^{-k_2\nu}\right) = K_{loc}^{2/3} t^{-k_1}$. From this, we obtain that $\xi(p > p_c) = K_{loc}^{1/3}$. We renormalized the determined scaling factor $\xi(p)$ with $\xi(p = 0.108) = K_{loc}^{1/3} \approx (56.33)^{1/3}$.

Determining the relation between the critical exponents

In order to find the relation between the critical exponents ν and s for obtaining the scaling law, we considered different values for β, such that $s = \beta\nu$. Then, we determined the parameters k_1 and k_2 of Eq. (5) of the maintext, which are given by $k_1 = \frac{2\alpha'}{3}$ and $k_2 = \frac{\alpha'}{3\nu}$, where $\alpha' = \frac{3}{2+\beta}\alpha$. We followed the finite-time scaling procedure described in the maintext and in Refs. [40, 41] for different β. The Fig. 4 shows the different rescaled curves optimized for obtaining the best single curve for $\beta = 6.6$, 5.70, 1, 0.58, 0.15, 0, -0.39, and -0.71. We observed that the best overlap of all the experimental data to a single curve is for the case $\beta = 1$, which is shown in Fig. 4c and was shown in Fig. 2c of the maintext. Note that the critical phase transition would be lost for $\beta \lesssim 0$ (Fig. 4f-h). The limiting value $\beta = 0$ (Fig. 4f) matches with a condition where $p_c = 0$ and $s = 0$.

Acknowledgments

We thank J. Chabé, F. Hebert and E. Altman for fruitful discussions. This work was supported by the DFG through Su 192/24-1. G.A.A. acknowledges the support of the Alexander von Humboldt Foundation and of the European Commission under the Marie Curie Intra-European Fellowship for Career Development grant no. PIEF-GA-2012-328605.

* gonzalo.a.alvarez@weizmann.ac.il
† dieter.suter@tu-dortmund.de
‡ robin.kaiser@inln.cnrs.fr

[1] M. Lewenstein, A. Sanpera, V. Ahufinger, B. Damski, A. Sen(De), and U. Sen, Advances in Physics **56**, 243 (2007).
[2] I. Bloch, J. Dalibard, and W. Zwerger, Rev. Mod. Phys. **80**, 885 (2008).
[3] L. Amico, R. Fazio, A. Osterloh, and V. Vedral, Rev. Mod. Phys. **80**, 517 (2008).
[4] T. Lahaye, C. Menotti, L. Santos, M. Lewenstein, and T. Pfau, Rep. Prog. Phys. **72**, 126401 (2009).
[5] P. Hauke, F. M. Cucchietti, L. Tagliacozzo, I. Deutsch, and M. Lewenstein, Rep. Prog. Phys. **75**, 082401 (2012).
[6] N. Y. Yao, C. R. Laumann, A. V. Gorshkov, S. D. Bennett, E. Demler, P. Zoller, and M. D. Lukin, Phys. Rev. Lett. **109**, 266804 (2012).
[7] N. Y. Yao, C. R. Laumann, S. Gopalakrishnan, M. Knap, M. Mueller, E. A. Demler, and M. D. Lukin, arXiv:1311.7151 [cond-mat, physics:quant-ph] (2013).
[8] I. Georgescu, S. Ashhab, and F. Nori, Rev. Mod. Phys. **86**, 153 (2014).
[9] P. W. Anderson, Rev. Mod. Phys. **50**, 191 (1978).
[10] D. Basko, I. Aleiner, and B. Altshuler, Ann. Phys. **321**, 1126 (2006).
[11] V. Oganesyan and D. A. Huse, Phys. Rev. B **75**, 155111 (2007).
[12] M. Znidaric, T. Prosen, and P. Prelovsek, Phys. Rev. B **77**, 064426 (2008).
[13] A. Pal and D. A. Huse, Phys. Rev. B **82**, 174411 (2010).
[14] F. Jendrzejewski, A. Bernard, K. Müller, P. Cheinet, V. Josse, M. Piraud, L. Pezzé, L. Sanchez-Palencia, A. Aspect, and P. Bouyer, Nat. Phys. **8**, 398 (2012).

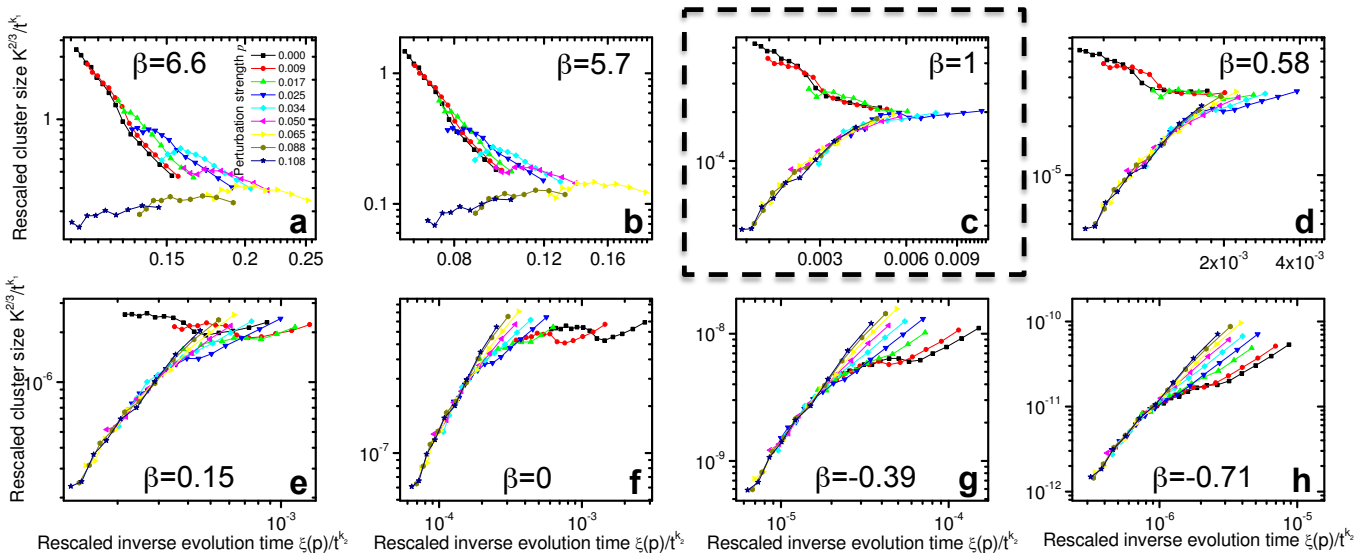

Figure 4. **Rescaled time evolution of the cluster size K after the finite-time scaling procedure for different perturbation strengths.** The rescaled experimental data of $K^{2/3}(t)/t^{k_1^{exp}}$ is shown as a function of $\xi(p)/t^{k_2^{exp}}$, where all curves overlap to the best possible single curve. The different panels from left to right, and from top to bottom show the rescaled curves for the shifted data points by $\xi(p)$ for $\beta = 6.6,\ 5.70,\ 1,\ 0.58,\ 0.15,\ 0,\ -0.39$, and -0.71 respectively. The best matching to a single curve is given when $\beta = 1$ and marked with a dashed line square (panel **c**). The critical transition would disappear for $\beta \lesssim 0$ (panels **f**-**h**).

[15] R. Vosk and E. Altman, Phys. Rev. Lett. **110**, 067204 (2013).

[16] G. Semeghini, M. Landini, P. Castilho, S. Roy, G. Spagnolli, A. Trenkwalder, M. Fattori, M. Inguscio, and G. Modugno, arXiv:1404.3528 [cond-mat] (2014), arXiv: 1404.3528.

[17] P. R. Zangara, A. D. Dente, A. Iucci, P. R. Levstein, and H. M. Pastawski, Phys. Rev. B **88**, 195106 (2013).

[18] S. Hofferberth, I. Lesanovsky, B. Fischer, T. Schumm, and J. Schmiedmayer, Nature **449**, 324 (2007).

[19] M. Rigol, V. Dunjko, and M. Olshanii, Nature **452**, 854 (2008).

[20] G. A. Álvarez, E. P. Danieli, P. R. Levstein, and H. M. Pastawski, Phys. Rev. Lett. **101**, 120503 (2008).

[21] A. Polkovnikov, K. Sengupta, A. Silva, and M. Vengalattore, Rev. Mod. Phys. **83**, 863 (2011).

[22] S. Trotzky, Y.-A. Chen, A. Flesch, I. P. McCulloch, U. Schollwöck, J. Eisert, and I. Bloch, Nat. Phys. **8**, 325 (2012).

[23] M. Cheneau, P. Barmettler, D. Poletti, M. Endres, P. Schauss, T. Fukuhara, C. Gross, I. Bloch, C. Kollath, and S. Kuhr, Nature **481**, 484 (2012).

[24] J. Schachenmayer, B. P. Lanyon, C. F. Roos, and A. J. Daley, Phys. Rev. X **3**, 031015 (2013).

[25] P. Jurcevic, B. P. Lanyon, P. Hauke, C. Hempel, P. Zoller, R. Blatt, and C. F. Roos, Nature **511**, 202 (2014).

[26] P. Richerme, Z.-X. Gong, A. Lee, C. Senko, J. Smith, M. Foss-Feig, S. Michalakis, A. V. Gorshkov, and C. Monroe, Nature **511**, 198 (2014).

[27] W. S. Bakr, J. I. Gillen, A. Peng, S. Fölling, and M. Greiner, Nature **462**, 74 (2009).

[28] J. Simon, W. S. Bakr, R. Ma, M. E. Tai, P. M. Preiss, and M. Greiner, Nature **472**, 307 (2011).

[29] R. Blatt and C. F. Roos, Nat. Phys. **8**, 277 (2012).

[30] J. W. Britton, B. C. Sawyer, A. C. Keith, C.-C. J. Wang, J. K. Freericks, H. Uys, M. J. Biercuk, and J. J. Bollinger, Nature **484**, 489 (2012).

[31] M. Saffman, T. G. Walker, and K. Molmer, Rev. Mod. Phys. **82**, 2313 (2010).

[32] B. Yan, S. A. Moses, B. Gadway, J. P. Covey, K. R. A. Hazzard, A. M. Rey, D. S. Jin, and J. Ye, Nature **501**, 521 (2013).

[33] L. Childress, M. V. Gurudev Dutt, J. M. Taylor, A. S. Zibrov, F. Jelezko, J. Wrachtrup, P. R. Hemmer, and M. D. Lukin, Science **314**, 281 (2006), http://www.sciencemag.org/content/314/5797/281.full.pdf.

[34] P. Neumann, R. Kolesov, B. Naydenov, J. Beck, F. Rempp, M. Steiner, V. Jacques, G. Balasubramanian, M. L. Markham, D. J. Twitchen, S. Pezzagna, J. Meijer, J. Twamley, F. Jelezko, and J. Wrachtrup, Nat. Phys. **6**, 249 (2010).

[35] V. Dobrovitski, G. Fuchs, A. Falk, C. Santori, and D. Awschalom, Annual Review of Condensed Matter Physics **4** (2013), 10.1146/annurev-conmatphys-030212-184238.

[36] G. Waldherr, Y. Wang, S. Zaiser, M. Jamali, T. Schulte-Herbr??ggen, H. Abe, T. Ohshima, J. Isoya, J. F. Du, P. Neumann, and J. Wrachtrup, Nature (2014), 10.1038/nature12919.

[37] C. Slichter, *Principles of magnetic resonance* (Springer, 1996).

[38] G. A. Álvarez and D. Suter, Phys. Rev. Lett. **104**, 230403 (2010); Phys. Rev. A **84**, 012320 (2011).

[39] G. A. Álvarez, R. Kaiser, and D. Suter, Ann. Phys. (Berlin) **525**, 833 (2013).

[40] J. Chabé, G. Lemarié, B. Grémaud, D. Delande, P. Szriftgiser, and J. Garreau, Phys. Rev. Lett. **101** (2008).

[41] G. Lemarié, G., J. Chabé, J., P. Szriftgiser, J. Garreau, B. Grémaud, and D. Delande, Phys. Rev. A **80** (2009).
[42] W. Warren, S. Sinton, D. Weitekamp, and A. Pines, Phys. Rev. Lett. **43**, 1791 (1979).
[43] J. Baum, M. Munowitz, A. N. Garroway, and A. Pines, J. Chem. Phys. **83**, 2015 (1985).
[44] S. Lacelle, Adv. Magn. Opt. Res. **16**, 173 (1991).
[45] R. Metzler and J. Klafter, Physics Reports **339**, 1 (2000).
[46] F. J. Wegner, Z. Physik B **25**, 327 (1976).